TECHNICAL REPORT STANDARD TITLE PAGE

1. Report No.	2. Government Accession No.	3. Recipient's Catalog No.
Final Report		

4. Title and Subtitle	5. Report Date
A Study of Acoustic Heating and Forced Convection in the Solar Corona	April 11, 1980
	6. Performing Organization Code

7. Author(s)	8. Performing Organization Report No.
Peter V. Foukal	

9. Performing Organization Name and Address	10. Work Unit No.
Atmospheric & Environmental Research, Inc. 872 Massachusetts Avenue Cambridge, Massachusetts 02139	11. Contract or Grant No. NAS8-32985
	13. Type of Report and Period Covered Final Report 1/1/79 - 4/1/80
12. Sponsoring Agency Name and Address George C. Marshall Space Flight Center, Marshall Space Flight Center, Alabama 35812	14. Sponsoring Agency Code AP 29-B

16. Abstract

We present the scientific objectives, data reduction, theoretical modelling, results, and conclusions of our investigation. In our study on the thermodynamics of magnetic loops in the solar corona, we use S055 EUV spectra to perform emission-measure and line intensity ratio analyses of loop plasma conditions. We discuss the evidence that loops contain plasma that is hotter than the background corona, and thus, require enhanced local dissipation of magnetic or mechanical energy. Our study of physical conditions in cool ultraviolet-absorbing clouds in the solar corona, uses the S055 EUV raster pictures, and optical data to derive constraints on the dimension, time scales and optical depths in dark opaque clouds not seen in Hα and CaK as filaments or prominences. From modelling, we find that these structures are exceptionally dense and cool coronal clouds with very steep temperature gradients to the surrounding corona. In our theoretical modelling of propagation of magnetically guided acoustic shocks in the solar chromosphere, we find that even in an inhomogeneous, static model; it is still unlikely that high frequency acoustic shocks could reach the solar corona. In our study on a dynamical model of spicules, we show, however that such guided slow-mode shocks can explain the acceleration of cool spicular material seen high in the corona.

17. Key Words (Selected by Author(s))	18. Distribution Statement
acoustic shocks coronal heating plasma diagnostics	

19. Security Classif. (of this report)	20. Security Classif. (of this page)	21. No. of Pages	22. Price*

*For sale by the Clearinghouse for Federal Scientific and Technical Information, Springfield, Virginia 22151.

(NASA-CR-161454) A STUDY OF ACOUSTIC HEATING AND FORCED CONVECTION IN THE SOLAR CORONA Final Report, 1 Jan. 1979 - 1 Apr. 1980 (Atmospheric and Environmental Research) 51 p HC A04/MF A01 CSCL 03B G3/92

N80-25263

Unclas 20987

Contents

1. Introduction

The program of study described in this report addresses two broad topics. Our first objective was to apply the most powerful spectral and radiative transfer diagnostic techniques to the S055 data on magnetic loops and dark absorbing structures, so as to place new limits on physical conditions in the plasma. Our second aim was to investigate, through numerical modelling of magnetically guided acoustic shock waves, to what extent slow mode shocks could explain the spicule and fibril phenomenon, and elucidate the injection of mass and energy into the solar corona.

One paper, co-authored by P. Foukal and J. Raymond is entitled "On the Thermodynamics of Magnetic Loops in the Solar Corona." It describes the reduction of S055 spectra of coronal loop structures, and their interpretation in terms of temperature, density and thermal equilibrium diagnostics in the loop plasma. The main thrust of this paper is to discuss critically to what extent high radiative losses in the coronal plasma, are to be interpreted as evidence for enhanced magnetic heating of these volumes.

A second study focusses on the detailed physical conditions in the remarkable dark absorbing clouds visible in the corona on S055 EUV raster pictures, but not generally visible in optical H_α or CaK photoheliograms. This work utilizes the large non-LTE computer code developed at SAO by E. Avrett, to study radiative transfer in the solar atmosphere. A paper is being prepared for submission with

J. Raymond and E. Avrett at the Center for Astrophysics. J. Raymond has acted as a paid consultant to AER, Inc., on these first two studies.

A third paper entitled "Propagation of Magnetically Guided Acoustic Shocks in the Solar Chromosphere" discusses our basic approach to handling acoustic shocks in a specific, inhomogeneous model of the chromosphere and magnetic geometry. The main result is that even in an inhomogeneous static chromosphere, it is difficult to transmit acoustic shocks with sufficient efficiency, to heat the corona. This paper has been accepted for publication in "Solar Physics." It was written in collaboration with M. Smart, who was employed at AER, Inc., under this contract during the summer of 1979, after completing his senior honours thesis at Harvard on this subject, under my direction.

A fourth paper, entitled "A Dynamical Model of Chromospheric Spicules, and Their Influence on the Mass and Energy Balance of the Solar Corona" is in preparation. This paper extends the results of the Foukal and Smart study to a moving atmosphere, and develops a specific model of spicule and fibril formation. This work has been carried out with the assistance of A. Munshi, a Harvard student employed at AER, Inc. in a part-time capacity, under this contract.

In section 2 the data reduction, modelling and results are described in more detail. In section 3 we draw some useful conclusions from the study as a whole, and suggest several fruitful directions for future work.

2. Data Reduction, Theoretical Modelling and Results

a) Thermodynamics of Magnetic Loops in the Solar Corona

i) Introduction

The observation that coronal radiative losses from magnetic active regions are typically enhanced by an order of magnitude compared to the quiet sun, is often cited as evidence that heating, that is; dissipation of mechanical or electrical energy, is higher in these regions.

In fact, this deduction is only reasonable if the higher losses can be proven to originate in a volume of higher plasma temperature T_1, relative to the lower temperature T_2 of the surrounding corona. In that case, the second law would rule out the conduction or advection of heat from T_2 to T_1, to balance the radiative losses. This would then necessitate a locally increased deposition of energy derived from dissipation of e.g. electric currents (Shklovskii 1965 Gold 1967, Rosner et al 1978) Alfven waves (Alfven 1947, Wentzel 1978, Ionson 1978) or channeled acoustic waves (Osterbrock 1961, Foukal and Smart 1980).

In practice, it has proven difficult to demonstrate the requirements of thermal equilibrium and $T_1 > T_2$, except in flares, where lines of e.g. FeXXIV demonstrate $T_1 \gtrsim 10^7 \gg T_2$. In general, the real error bars on plasma temperatures derived in active region loops and background corona (e.g. Pecker et al 1954, Firor and Zirin 1963, Mason 1975 Gabriel and Jordan 1975) exceed the quoted differences $\Delta T = T_1 - T_2$.

In this study, we bring to bear upon this problem, a detailed analysis of the rich EUV line spectrum of several bright loops observed with the S055 spectrometer during the ATM missions. To the best of our knowledge, this analysis is the first instance where S055 spectrometer pointings and wavelength scans have been located in well-defined loops at the limb. We apply emission measure analysis, and also line intensity ratios to study a) the thermal equilibrium of loop plasma b) the temperature distribution of plasma in the loop relative to outside corona c) the density and element abundances in the loops.

ii) Data and Reduction

Through examination of the full S055 data base of spectra taken between June 1973 and January 1974, we were able to find three sets of spectra in which the pointing was definitely within a loop off the limb and not contaminated by disc features. The pointing information for the 5 x 5 arc sec spectrometer aperture was obtained from the ATM H_α atlas, and also from large-area S055 raster pictures in ultraviolet radiations, in which the aperture could be located directly, to within 5 x 5 arc sec.

Fig. 1 illustrates sample rasters of loops, in ultraviolet lines covering the range of plasma temperature between 1.5×10^5 K (OIV554) to 1.6×10^6 K (MgX 625). The locations of the spectrometer aperture are shown by small dark circles.

A total of 9 full spectra of high quality, were taken at these pointings, covering in each case the spectral range 280 - 1340 A°, with 1.6 Å spectral resolution. Our first step in reduction of the spectra, was to identify the various ultraviolet lines of interest, including several weak emissions in the temperature range $T > 10^5$ K, never before used as solar plasma diagnostics.

Calibrated intensities were then derived, for the lines listed in Table I, using the updated calibration of Reeves et al (1977).

iii) Results

The emission measure defined as;

$$EM(T) = \int_{0.891T}^{1.122T} N_e N_H \, dh$$

was calculated, assuming constant gas pressure, from the absolute intensity in each line. The curves of EM(T) averaged over the spectra in each loop, are plotted in Fig. 2 for each of the three loops. For comparison, a fourth curve gives the emission measure distribution derived by us from the averaged quiet corona line intensities published from the S055 spectra by Vernazza and Reeves (1978).

As a measure of the error in the emission measure curves, we have used an equilibrium-excitation and ionization code (Doyle and Raymond 1980) to calculate the predicted line intensities from this emission measure distribution, for comparson (Fig. 3) with the observed values. It is seen that agreement is generally quite good--to within about a factor two.

Table I

Intensities (ergs $cm^{-2} s^{-1} sr^{-1}$) of Lines Measured

Ion	λ Å	Jan 7	Jan 8	Jan 5
CII	1335	244	1.3	366
	904	4	--	--
CIII	1176	25	--	93
	977	66	4	150
NII	1085	15	--	13
NIII	991	10	--	10
NIV	922	4.5	--	--
	764	32	3	25
NV	1240	65	38	93
OII	702	17	2	20
OIV	789	106	16	81
	554	112	13	63
OV	760	42	7	30
	630	372	75	330
OVI	1034	1135	614	1546
NeIV	468	19	--	--
	542	18	--	--
NeV	570	33	4	17
	481	31	--	31
NeVI	560	49	11	60
	434	207	50	247
NeVII	895	21	20	20
	465	259	104	268
NeVIII	775	242	222	238
MgVI	401	<590	--	--
MgVII	434	286	177	209
MgVIII	436	276	235	238
MgIX	706	15	24	33
MgX	615	482	621	659
SiIII	1206	124	--	67
SiIX	950	7	16	5
SiXI	581	23	42	66
SiXII	505	531	850	1092
SVI	937	42	23	38
SXIV	425	165	248	170
FeXVIII	974	5	7	9
FeXX	805			

Deviations of the ratio plotted in Fig. 3 from unity are a measure of primarily, abundance errors and departures from ionization and excitation equilibrium in the loop plasma.

Two main points emerge from the relative shape of the three loop curves in Fig. 2, as compared to the background emission measure curve; a) the loop curves do not turn over at higher temperature log $T \geq 6.5$, as rapidly as the background curve. This suggests that there may be relatively more hot plasma in these structures than in the quiet corona, b) there is also a lot more cool plasma at $T < 10^6$ K, well above the limb in these loops, than in the quiet corona.

Point (a) shows that even sunspot-type loops, visible most prominently in lines such as OIV, OVI and NeVII show a small emission-measure excess at coronal temperatures. This certainly supports the view that loops in general exhibit regions of relatively high losses from $T > 10^6$ K plasma radiations. However, we stress, and it can be seen from Fig. 2, that it is exceedingly difficult to demonstrate from emission measure analysis alone, that higher plasma temperatures are actually achieved in the loops than in the background.

Table II shows the results obtained from the line intensity ratios, that we have used to indicate departure from thermal equilibrium in the plasma. The line intensity ratios given span the temperature range roughly 6×10^4 K to 7×10^5 K. Comparison of the values obtained in our loops, with the ratio calculated from our model for the case of thermal

equilibrium, gives an estimate of departure from thermal equilibrium. This difference is indicated by the disparity between the temperature at which the lines are actually formed, and the temperature at which the ion should be formed, if thermal equilibrium were rigorously maintained.

TABLE II

Ion	Line Ratio	Loop	Background	Model	log T_{lines}	Log T_{ion}
NeVII	$\frac{I(895)}{I(465)}$	0.079	0.045	0.038	5.40	5.75
NeVII	$\frac{I(562)}{I(465)}$	0.059	-	0.078	<5.75	5.75
OIV	$\frac{I(554)}{I(789)}$	1.05	1.25	1.24	5.15	5.20
OIII	$\frac{I(508)}{I(702)}$	0.48	0.43	0.51	4.90	4.90

In general, we see from the difference in the last two columns, that the lines tend to be formed at lower temperatures, i.e. log T_{lines} < log T_{ion}. This is consistent with the situation found in our model, when a plasma is allowed to cool rapidly from coronal temperatures. This supports the view (Foukal, 1976, 1978) that the cool loop plasma is coronal material condensing and cooling to chromospheric temperatures. This result is supported also by our preliminary analysis of several other line-intensity ratios, for which atomic parameters are less certain, and which we have thus not included in Table II.

b) Physical Conditions in Cool Coronal Clouds

i) Introduction

Optical observations in the H_α and CaK lines show that large volumes within the hot ($T > 10^6$ K) coronal medium are occupied by much cooler $T \sim 10^4$ K plasma. This cool material is localized in discrete regions seen in H_α and CaK as dark filaments on the disk, and as bright prominences on the limb. It has been shown in previous EUV studies (e.g. Schmahl et al 1974, Orrall and Schmahl 1976) that this material is optically thick in the Lyman continuum, at $\lambda <$ 912 Å.

The hot ($T > 10^6$ K) coronal medium between these filaments and prominences is conventionally taken to be optically thin in the ultraviolet. This assumption is essential to physical analyses of solar and stellar coronae (e.g. Pottasch 1963, Withbroe and Noyes 1977).

But several analyses of ultraviolet data (Withbroe 1970, Kanno 1979, Foukal 1978, Schmahl and Orrall 1979) show evidence for important absorption by neutral hydrogen outside these discrete optical features. In a previous paper (Foukal 1978) we showed very dark, discrete absorbing structures in S055 raster pictures taken in EUV lines and continua. In this study we have analysed additional S055 ultraviolet data on these dark coronal "clouds," and also compared them with good quality optical data. We also used a non-LTE radiative transfer model to study the physical conditions in these structures, and relate them to coronal dynamics.

ii) Data and Reduction

The data used in this study were polychromatic EUV raster pictures from the S055 spectrometer. The S055 rasters taken between June 1973-January 1974 were searched for distinct dark structures in EUV radiations. Four examples of these dark clouds are given in Figs. 4, 5, 6, 7. We see distinct dark structures ranging morphologically between an arcade of parallel fibrils or low magnetic loops (Fig. 4), an irregular "cloud" over plage (Fig. 5), an active region filament-like structure (Fig. 6), and a time series of a loop-like structure (Fig. 7). To examine the optical appearance of these EUV dark clouds, we obtained the best quality H_α photopeliograms and CaK spectroheliograms from Big Bear and Sacramento Peak. These were scaled and oriented similarly to the EUV pictures, and are also shown in Fig. 4-6.

We note that in general, there is no evidence for prominent dark optical structures, such as active region filaments, at the location of the distinct EUV clouds. Conversely, dark active region filaments (e.g. Fig. 5) seen prominently in H_α are not always visible in the EUV radiations, or in CaK, although they can appear dark in some cases not illustrated here.

As we pointed out in our previous paper (Foukal 1978), the opacity of EUV clouds at wavelengths such as λ977, λ1032, λ1335 located longward of the Lyman continuum edge cannot be explained in terms of neutral hydrogen. The opacity at λ1335 is likely to be caused by resonance scattering in the core of the strong resonance line of CII at that wavelength.

However, at λ977, λ1032 we require a source of continuum opacity never before considered in connection with the optical depth of the hot corona. This opacity source is CI, particularly its $2p^2\ {}^3p$ continuum, with an edge at $\lambda_\infty = 1100\text{Å}$.

The rasters also yield useful information on the dimensions, height over the photosphere, and lifetimes of the EUV clouds. The basic observational constraints are summarized in Table III. Our objective in modelling these structures was to determine the simplest model that would explain these constraints in a physically reasonable and self-consistent manner. It is beyond the scope of our analysis to establish the uniqueness of this model, although we do compare our results with some of the closely studied models of active region filaments and prominences.

In our modelling of these optically thick clouds, we used the non-LTE radiative transfer code "Pandora" developed at SAO for studies of the solar photosphere and chromosphere (Vernazza et al 1973). Our basic physical model is illustrated in Fig. 8a. It is a plane parallel infinite slab lying in the xy plane, suspended magnetically above the photosphere at a height of 20,000 km, with the Z-axis normal to the local solar photospheric surface. The density ρ in the slab is taken constant, with magnetic stresses assumed to balance any pressure gradients arising from temperature gradients in the Z-direction. We then use the Pandora code to calculate the ionization structure, opacity in HI and CI, CaII lines and continua, and emergent fluxes in various strong lines, such as Lyα and CII 1335, Hα and CaK.

Table III.

Summary of Observational Constraints

1.	Morphology in EUV radiations:	Distinct dark loops, filamentary structures, or irregular shapes.
2.	Characteristic Horizontal Scale:	$L \lesssim 5 \times 10^4$ km
3.	Characteristic Vertical Scale:	$h < 1 \times 10^5$ km
4.	Characteristic Thickness in Vertical Direction:	$\Delta h \lesssim 1 \times 10^4$ km
5.	Optical Depth $\tau(\lambda)$:	$\tau(\lambda) \gtrsim 1$ at; $\lambda\lambda$1335, 1216, 1032, 977, 896, 625, 554. $\tau(\lambda) < 1$ at; CaII K-line, Hα.
6.	Brightness Contrast $C(\lambda)$ relative to surroundings:	$C(\lambda) << 1$ at $\lambda\lambda$ 1335, 1216, 1032, 977, 896 and 554 $C(\lambda) \sim 1$ at λ625, CaII K-line, Hα.

iii) Results

After several adjustments of the model primarily dictated by the need to produce high column density of CI, but low column densities in CaII and in the n=2 population of HI, we have found a temperature profile T(Z), and density in the slab, illustrated in Fig. 8b. The temperature gradient at $T > 3 \times 10^4$ K is very large, and is determined by the constraint that transition region emissions (e.g. CIII 977, OIV 544, OVI 1032) are very weak, even though the density in the very dark structures is very high (Dupree, Foukal and Jordan 1976).

Overall, our calculations show a very cool ($T \lesssim 6 \times 10^3$ K) gas in the central regions, with an exceptionally steep temperature gradient to coronal temperatures. Comparison with conditions in prominences (e.g. Orrall and Schmahl 1976) and active region disc filaments (e.g. Tandberg-Hansen 1971) indicates that the EUV clouds are even denser than these optical structures, and the temperature jump from very cool plasma ($T \lesssim 8 \times 10^3$ K) to coronal values ($T > 10^6$ K) is much (at least a factor 10 at 1×10^4 K $< T < 3 \times 10^5$ K) steeper.

We suggest, from the comparable lifetimes of the EUV clouds, and their diverse morphology, that they are not a particular and separate class of coronal structures. Rather, we believe them to be simply situations in which the isobaric condensation (e.g. Kleczek 1958) of coronal matter in filaments, fibrils, and loops has achieved exceptionally high densities and correspondingly very low temperatures.

c) Propagation of Magnetically Guided Acoustic Shocks in the Solar Chromosphere

i) Introduction

The most attractive mechanism for heating of the outer solar atmosphere above the temperature minimum has been dissipation of acoustic shock wave energy. This mechanism (Biermann 1946, Schatzmann 1949) utilizes the observed turbulence at the solar photosphere to generate sound waves that then steepen to shocks. Both the generation of the sound and the propagation and dissipation of the shocks can be treated using relatively well-understood fluid properties.

However, recent observations from the OSO-8 satellite (Athay and White 1978, Bruner 1978) have shown that there is insufficient power ($\lesssim 1 \times 10^4$ ergs cm^{-2} sec^{-1}) in travelling waves at periods P $\gtrsim$ 40 secs, to balance measured coronal losses. This makes it unlikely that these long-period waves are responsible for coronal heating. At the same time, acoustic shock calculations (Ulmschneider 1971, Bird 1964b) have shown that in a plane parallel static atmosphere, short period (P $\lesssim$ 50 secs) waves will be dissipated in the chromosphere, well before even reaching the corona. Thus the OSO-8 observations at P $\gtrsim$ 40 secs, and this theoretical result for P $\lesssim$ 50 sec waves would, when taken together appear to rule out coronal heating by acoustic shock waves of <u>any</u> period.

However, observations sensitive to short acoustic wave frequencies P < 40 secs (Deubner 1976, Athay and White 1979) do show possibly very large flux densities at these

high frequencies, around the temperature minimum. It then becomes of considerable interest whether the theoretical result derived for plane parallel, static chromospheres also holds for a more realistic (ie inhomogeneous, moving) chromosphere.

In this study, we have integrated the shock propagation equations through a static, but inhomogeneous chromosphere. Specifically, we determine the propagation and dissipation properties of acoustic (slow mode) shocks guided along the field lines of the intense and rapidly diverging magnetic field in the chromospheric network.

ii) Equations and Model Atmosphere

The propagation of an acoustic shock through a gravitational atmosphere has been treated by the method of characteristics for several cases of relevance to the solar atmosphere by Bird (1964a) and by Kopp (1968). A total differential equation is derived, relating the shock strength $\alpha = M_s - 1$ or Mach number M_s, to variations in the density ρ, temperature T, and flow cross-section A, ahead of the shock.

For the special case of a periodic train of weak shocks in a static atmosphere, the shock propagation equation takes the form;

$$\frac{1}{\alpha}\frac{d\alpha}{dX} = \frac{1}{2}\left\{-\frac{1}{a_o}\frac{da_o}{dX} + \frac{\gamma g}{a_o^2} - \frac{1}{A}\frac{dA}{dX} - \frac{4\alpha}{a_o P}\right\}$$

Here a, g, P, γ represent respectively the sound speed, acceleration of gravity, shock period, and the ratio C_p/C_v

of specific heats. The subscripts o and 1 denote values ahead of, and behind the shock.

A detailed consideration of the various terms on the right hand side has been given in our paper (Foukal and Smart 1980). The basic procedure in this analysis was to calculate an initial shock strength α_o at an initial height $X = X_o$ in the atmosphere, and then to integrate this equation numerically, using a finite difference scheme, taking $a_o(X)$ as given by a chromospheric model e.g. (Vernazza, Avrett and Loeser 1973, Kopp 1968) and using a model of the magnetic field geometry, to determine $\frac{1}{A}\frac{dA}{dX}$.

Our model of the magnetic field lines was obtained by solving the magneto-static equilibrium relation;

$$\nabla p = \vec{J} \times \vec{B} ,$$

which was reduced to a balance between the external gas pressure $p(h)$ and the magnetic pressure $B^2(h)/8\pi$, at every height h above X_o. The profile of A(h) is given in Table IV.

The calculations were performed both at constant $\gamma = 5/3$, and with γ variable. The atmospheric model of T, ρ and γ that we used in our integrations is given in Fig. 9.

iii) Results

To check the treatment of shock wave propagation and dissipation used here, we first compared our results for a plane parallel ($\frac{1}{A}\frac{dA}{dX} = 0$) atmosphere with Ulmschneider's (1971) previous calculations. For these runs, we used values

TABLE IV

Magnetic Geometry

Height (km)	Radius (km)	Area (km^2)
below 750	170	9.4×10^4
at 900	690	1.5×10^6
1200	1730	9.4×10^6
1500	2770	2.4×10^7
1800	3810	4.6×10^7
2000	4500	6.4×10^7
above 2000	4500	6.4×10^7

of α_o, and $a_o(X)$ similar to his computations, in which the shock propagation and dissipation were treated quite differently. The results are given in Fig. 10, for shocks of 15 and 50 secs period. It can be seen that the agreement is good, namely, the flux density remaining in the shock as a function of height is closely similar. If anything, Ulmschneider's code predicts higher losses than ours.

In Fig. 11, we show the losses suffered in a wave propagating up a diverging magnetic flux tube. Here the relative losses are much less. Even the 15 sec wave, the most heavily attenuated, retains fully 70% of its flux density to 1500 km above the height of shock formation. However the results of Fig. 11 are obtained at relatively low initial shock strengths α_o. Although the transmission is high, the total flux, integrated over all flux tubes in the network, is still too low by a factor 70, to heat the corona. The reason is that the fractional area of the photosphere covered by the flux tubes is only (e.g. Stenflo 1976) about 1×10^{-3}.

Fig. 12 shows what happens if we attempt to make up for the small fractional area, by increasing the acoustic flux density (ie α_o) in each magnetic tube. Once again, the transmission drops, so that the transmitted total flux emitted globally into the corona, is always too small to balance its observed losses.

Our conclusions are; a) diverging magnetic fields may well redistribute acoustic flux dissipation vertically,

relative to non-magnetic photosphere and this could be a factor in determining the vertical temperature profile of network magnetic flux tubes, and also plages. b) the global acoustic flux that penetrates even an inhomogeneous, static atmosphere is unlikely to be sufficient for heating the corona.

d) A Dynamical Model of Chromospheric Spicules, and of Their Influence on the Mass and Energy Balance of the Solar Corona.

i) Introduction

The most promising mechanism for accelerating spicules was originally put forward by Osterbrock (1961) and Uchida (1961). It associates spicules and active region fibrils with the perturbation in temperature, density and velocity behind a slow-mode (acoustic) shock guided through the chromosphere by magnetic fields of e.g. the network. Wentzel and Solinger (1967) showed that in a uniform vertical magnetic field, a shock of plausible initial strength can produce temperatures and densities close to spicular values, when the gas velocity behind the shock is roughly 20 km sec^{-1}, as observed in spicules. But that study did not consider the important influence of rapidly diverging magnetic field lines on the shock propagation. More generally, no attempt was made to explain the most basic and troublesome observation, namely; how does such cool and dense gas get so high into the corona, well above the ballistic trajectory h calculated from the observed velocities, that is, $h >> \frac{u^2}{2g}$.

In this study, we use the shock propagation equations described in sect (c) above, to construct a reasonable dynamical model of the spicule phenomenon.

ii) Equations, Physical Model, and Results

To calculate the propagation of the acoustic shock along diverging magnetic field lines, we used a similar propagation equation to that described in sect (c) above, but without the dissipative term, of the form $4\alpha/a_o P$, that describes damping of the shock by its own wake. The reason for neglecting this term is that its ratio to other terms in the equation scales as $1/_P$, where P is the shock wave period. For the high frequency shocks discussed in (c), the term is important. But for long period disturbances ($P \gtrsim 300$ secs) that would generate spicules, the term is negligible. As a first step in the actual calculation, we derive an initial Mach number M_s at the height $h \sim 750$ km, where Ulmschneider's (1971) simple wave computation indicate the shocks will form. Judging from the velocities observed in granulation, this Mach number will be in the range 1.1 - 1.8.

The propagation equation is then integrated upward through the diverging magnetic field geometry that was calculated from magneto-hydrostatic equilibrium in sect (c) above (see Table IV). Using the values of $M_s(h)$ from the propagation equation, it is then a simple matter to calculate the gas flow velocity u_1, sound speed a_1, and density ρ_1, immediately behing the shock, using the standard jump relations (e.g. Landau and Lifshitz 1959).

The results are given in Figs. 13, 14, 15. We note in particular, that the shock Mach number M_s drops around $h \sim 1000$ km, due to the diverging field lines, and then recovers when the field lines become parallel. The gas immediately behind the shock is accelerated powerfully, to outward velocities that reach 65 km sec^{-1} at $h = 1 \times 10^4$ km, behind the stronger of the two shocks shown. The gas temperature, calculated from the sound speed a_1, is about 1.6×10^5 K, and the particle density is $1.2 \times 10^8 cm^{-3}$.

We then calculate the cooling time of this plasma, after the shock has passed. The energy equation is;

$$\rho c_p \frac{dT}{dt} = -n_e n_H \phi(T)$$

Here $\phi(T)$ is the radiative loss function for plasma of solar elemental abundances, as given e.g. by McWhirter et al (1975). This yields for the cooling time, t_c, from the temperature T, behind the shock, to the observed spicular temperature T_s;

$$\int_o^{t_c} dt = \frac{\gamma}{\gamma-1} \frac{R}{\mu} M_H \int_{T_s}^{T_1} \frac{\phi(T)^{-1}}{n_e} dT.$$

If we assume, reasonably enough, that the plasma will cool isobarically, we can evaluate this integral, to yield;

$$t_c = \frac{9.5 \times 10^{-10}}{P_1} \int_{T_s}^{T_1} T dT \sim 10^2 \text{ secs}$$

At the same time, the deceleration time t_D under solar gravity, of this cooling gas is;

$$t_D = U_1/g \sim 250 \text{ secs}$$

We thus have shown that the gas will cool rapidly to a temperature where it will become visible in H_α and other optical radiations. The decelerated, cooled and condensed gas that is seen in these radiations as a spicule will have an outward velocity of the order of 10 km sec^{-1}, a temperature $T \sim 1.5 \times 10^4$ and a density $P_1/2kT_s \sim 10^{10}$ cm^{-3}, as observed (e.g. Beckers 1972).

3. Overall Conclusions and Suggestions for Further Work

The data analysis and theoretical modelling performed under this contract have led to a number of interesting conclusions, that advance our knowledge of coronal dynamics.

For one, our calculations of acoustic shock guiding have demonstrated how diverging magnetic fields in the network and plages can significantly increase the local transmission efficiency of acoustic power within the intense flux tubes. This opens up a new physical mechanism for heating chromospheric plages, that uses direct observations of velocity fields in the photosphere, direct observations (e.g. Giovanelli, 1980 private communication) of field line divergence, and relatively well understood properties of acoustic shocks. On the other hand, our calculations also showed that even in an inhomogeneous model of the chromosphere, it appears unlikely that the global transmission efficiency of high frequency acoustic power is sufficient to heat the corona. In this sense, our calculation strengthens the result (Athay and White, 1978) that acoustic shocks are not the primary heating source of the corona.

Another clear result of our shock wave investigation, is that an exceedingly attractive model of spicule temperature, density and velocity, can be calculated, using the acceleration of low coronal material by an acoustic shock of plausible (weak) strength, and then comparing its cooling time to its deceleration time under gravity.

Our study of shock waves guided along magnetic field lines suggests a number of fruitful directions to follow in the future. For one, it would be a relatively simple matter to use our shock wave dissipation functions to calculate the relative temperature profile above the temperature minimum in the chromosphere, in a region of diverging fields, and in a non-magnetic region. It would be interesting to compare such a profile with empirical models of faculae and plages (e.g. Chapman, 1970, Shine and Linsky, 1974).

Another question posed by our results is what are the propagation characteristics of high frequency acoustic shocks in the moving medium represented by upwardly accelerated spicules? The framework for such a calculation is available in the propagation equations we have used. However a treatment including motions ahead of the shock requires explicit evaluation of complex non-adiabatic terms. We hope to address this question in the future, using accurate cooling rates for chromospheric gas, presently being calculated by Avrett at SAO.

The work we have performed under this contract on plasma temperature and density in loops has also laid the basis for a critical study of the thermodynamics of these loops. We have completed analysis of all the S055 spectra relevant to the investigation, carried out the emission measure analysis, and also most of the analysis of line intensity ratios. Our results indicate that there is indeed evidence to believe that enhanced energy deposition takes place in loops, since

the plasma temperature does seem to achieve higher values than in the background. We now are running final model calculations, using new atomic cross-sections recently made available from the Belfast group, to complete the line intensity-ratio analysis, before publishing our conclusions. We expect that our results will yield the first proper demonstration that active regions are in fact "hotter", and point out the thermodynamic consequences of this result.

Finally, our analysis of cool absorbing clouds has yielded a physically consistent picture of the density and temperature conditions in these remarkable structures. Our identification of these structures in the S055 rasters has given new evidence for the existence of large opacity by cool gas in the coronal medium, established the basic physical conditions in these structures, and laid the basis for eventual understanding of their dynamics. The recognition that opacity is present even longward of $\lambda 912$ Å, has important implications for the use of plasma diagnostics in loops and other active region coronal structures. The close proximity of the ultra-cool material to sunspots confirms our previous evidence that the corona over sunspots is in general a region of anomalously <u>low</u> temperature, so that the coolness of an umbra extends right through the photosphere, chromosphere and to at least 50,000 km in the corona.

We acknowledge valuable assistance in our work from E. Avrett at SAO, whose calculations using the Pandora code have

been of great assistance in analyzing conditions in the cool clouds. Also R. Moore at BBSO and S. Hinata at SPO have helped us in providing H_α photoheliograms and CaK spectroheliograms that we have used in that same analysis.

4. References

Alfvèn, H. (1947) Mon. Not. Roy. Astr. Soc 107, 211.

Athay, G., and White, O. (1978) Ap. J. 226, 1135.

Athay, G., and White, O. (1979) Ap. J. Suppl. 39, 333.

Beckers, J. (1972) Ann. Rev. Astr. Ap. 10, 73.

Biermann, L. (1946) Naturwiss. 33, 118.

Bird, G. (1964a) Ap. J. 139, 675.

_____ (1964b) Ap. J. 140,288.

Bruner, E. (1978) Ap. J. 226, 1140.

Chapman, G. (1970) Sol. Phys. 14, 315.

Deubner, F. (1976) Astron. Ap. 51, 189.

Doyle, R. and Raymond, J. 1980 in preparation.

Dupree, A., Foukal, P., and Jordan, C. (1976) Ap. J. 209, 621.

Firor, J. and Zirin, H. (1965) Ap. J. 135, 122.

Foukal, P. (1976) Ap. J. 210, 575.

Foukal, P. (1978) Ap. J. 223, 1046.

Foukal, P., and Smart, M. (1980) Sol. Phys, in press.

Gabriel, A. (1976) Phil. Trans. Roy. Soc. London A281, 339.

Gabriel, A. and Jordan, C. (1975) Mon. Not. Roy. Astr. Soc. 173, 397.

Gold. T. (1968) in Proceedings of the Ninth Nobel Symposium, Y. Ohman, ed.

Hinata, S. (1979) Ap. J. 232, 915.

Ionson, J. (1978) Ap. J. 226, 650.

Kanno, M. (1979) Publ. Astr. Soc. Japan. 31, N°1.

Kleczek, J. (1958) Bull. Astr. Inst. Czech. 8, 120.

Kopp. R. (1968) unpublished PhD thesis, Harvard Univ.

Landau, L. and Lifshitz, E. (1959) Fluid Mechanics, Pergamon Press.

Mason, H. (1975) Mon. Not. Roy. Astr. Soc. 171, 119.

McWhirter, R., Thonemann, P. and Wilson, R. (1975) Astron Ap. 40, 63.

Orrall, F. and Schmahl, E. (1976) Solar Phys 50, 365.

Osterbrock, D. (1961) Ap. J. 134, 347.

Pecker, C., Billings, D. and Roberts, W. (1954) Ap. J. 120, 509.

Pottasch, S. (1963) Ap. J. 137, 945.

Reeves, E., Timothy, J., Huber, M. and Withbroe, G. (1977) Appl. Optics 16, 837, 849.

Rosner, R., Tucker, W. and Vaiana, G. (1978) Ap. J. 220, 643.

Schatzmann, E. (1949) Ann. Ap. 12, 203.

Schmahl, E., Foukal, P., Huber, M., Noyes, R., Reeves, E., Timothy, J., Vernazza, J., and Withbroe, G. (1974) Sol. Phys. 39, 337.

Schamhl, E. and Orrall, F. (1979) Ap. J. 231, 241.

Shine, R. and Linsky, J. (1974) Sol. Phys. 39, 49.

Shklovskii, I. (1965) Physics of the Solar Corona Addison-Wesley.

Stenflo, J. (1976) in I.A.U. Symposium N°7, eds. Bumba and Kleczek, p. 70.

Tandberg-Hansen, E. (1971) Solar Activity

Uchida, Y. (1969) Publ. Astr. Soc. Japan 21, 128.

Ulmschneider, P. (1971) Astr. Ap. 14, 275.

Vernazza, J., Avrett, E. and Loeser, R. (1973) Ap. J. 184, 605.

Vernazza, J. and Reeves, E. (1978) Ap. J. Suppl 37, 485.

Wentzel, D. and Solinger, A. (1967) Ap. J. 148, 877.

Wentzel, D. (1978) Revs Geophys. Space Phys. 16, 757.

Withbroe, G. (1970) Sol. Phys. 11, 208.

Withbroe, G. and Noyes, R. (1977) Ann Rev. Astr. Ap. 15, 363.

5. Captions

Fig. 1 Ultraviolet raster pictures of loops observed with the S055 spectrometer. The format of these mini-rasters, taken to provide pointing information for the spectra, is about 2' x 5'. In the vertical column on the left (January 5th), a loop structure and plume are seen in McMath 12690 on the SE limb at GMT 1711, in OIVλ554, OVIλ1032 and Mg Xλ625. The two top pictures in the right hand column show a bright plume over a spot in McMath 12694, at the E limb on January 7th GMT 14:20, in NeVIIλ465 and MgVIIIλ436. A loop in the same active region, on January 8th at GMT 01:13, is seen in the lower two frames, in the same two lines.

Fig. 2 Plot of emission measure against temperature for the three loops observed, and for "background" corona, over the temperature range 1×10^4 K < T < 5×10^6 K. The lines used are listed in Table I.

Fig. 3 Plot of observed intensities in the lines used to calculate emission measures in Fig. 2, divided by predicted intensities of those same lines, as calculated from the resulting plasma temperature distribution.

Fig. 4 Dark EUV absorbing material near active region McMath 12503 on August 28, 1973. The location of the dark structure is indicated by an arrow in the Lyman-alpha raster picture, taken at GMT 15:01. The same feature is seen also on rasters taken simultaneously in Lyman continuum λ896, and lines of CIIλ1335, CIIIλ977, OIVλ554 and OVIλ1032. The feature is <u>not</u> seen in MgXλ625. Arrows also indicate the location of the EUV dark feature, on optical photoheliograms in H_α (Big Bear photograph taken at GMT 15:13) and in CaK (taken at McMath-Hulbert at GMT 14:30). The optical pictures are printed to similar scale and orientation as the EUV rasters. The feature is <u>not</u> seen in these optical radiations.

Fig. 5 An irregularly shaped dark EUV absorbing structure in active region McMath 12507 on September 2, 1973. An arrow indicates the dark structure on the Lyman-alpha raster. It is also seen prominently on raster pictures, taken simultaneously at GMT 02:05, in resonance lines of CII, CIII, OIV and OVI. It is less visible in MgX radiation. No Lyman continuum observations were taken at this time. The closest available H_α photoheliograms were taken at Big Bear 2h 22 m before the EUV rasters, and 13h 21 m after-

ward. The location of the EUV structure is indicated by an arrow in the earlier H_α photo. The closest available CaK was taken at Sacramento Peak 11h 39 m after the EUV rasters. An arrow indicates the location of the EUV dark structure on this CaK frame.

Fig. 6 A dark EUV-absorbing structure in active region McMath 12535 on September 24, 1973, GMT 00:32. As in Figs. 1, 2, arrows indicate the location of the structure in the Lyman raster picture and show the location of the same area also in H_α and CaK photoheliograms. It is hardly visible in the MgX EUV raster. The two H_α pictures were taken 10h 02 m before (on left) and 8h 16 m after the EUV rasters. The CaK picture was taken at Sacramento Peak 13h 27 m after the EUV rasters.

Fig. 7 Time sequence of a dark loop-like EUV structure near active region McMath 12474 on August 7, 1973. Arrow indicates the structure in the CIIλ1335 resonance line, at t_o = GMT 04:08. It is shown at t_o also in radiations of OVI and OIV. Later frames of the sequence show the structure in these radiations 22m and 39m later.

Fig. 8 In (a) we illustrate the basic geometry of the slab model. In (b) we give the "best

fit" temperature distribution T(Z) derived from our iterations.

Fig. 9 The vertical profiles of temperature T, density ρ and the ratio of specific heats γ, for the principal model atmosphere used in these calculations. The density profiles were calculated on the assumption of hydrostatic equilibrium. In one case γ was held constant, in the other case it was allowed to vary as shown above.

Fig. 10 Curves of flux density F(h) remaining at a height h above $\tau_{0.5} = 1$, in a plane-parallel atmosphere of $\gamma = 5/3$. The curves shown here represent shocks of 50 second and 15 second periods. The curves designated U are from Ulmschneider (1971).

Fig. 11 Curves of flux A(h)F(h) remaining in a diverging magnetic flux tube, for shock periods of 15 s and 50 s. The initial flux values correspond to the same initial flux densities as in Fig. 2, but are multiplied by the cross-sectional area 9.4×10^4 km^2 of a network flux tube at h = 750 km.

Fig. 12 Curves of flux A(h)F(h) remaining in a diverging magnetic flux tube for a higher initial shock strength $\alpha_o = 0.3$. Shock periods of P = 15, 28 and 50 s are shown. The curves given are calculated with $\gamma = 5/3$, thus for highest transmission. The dashed curve was calculated with the model of Gabriel (1976).

Fig. 13 Plots of the shock Mach number M_s against height, h, above $\tau_{o.5} = 1$, for initial Mach numbers at h = 750 km of 1.4, 1.8.

Fig. 14 Plots of the density ρ_1 immediately behind the shock, against height, h, for initial shock Mach numbers of 1.4, 1.8.

Fig. 15 Plots of the sound speed a_1, and the gas velocity, u_1, directly behind the shock, against height, h, for two initial Mach numbers at h = 750 km; 1.4 and 1.8.

JAN 5

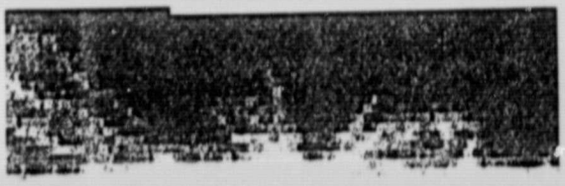

O IV

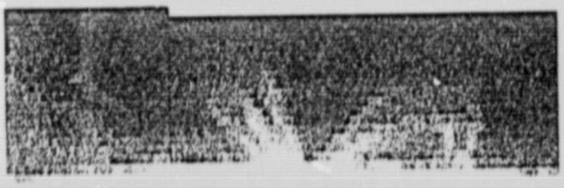

O VI

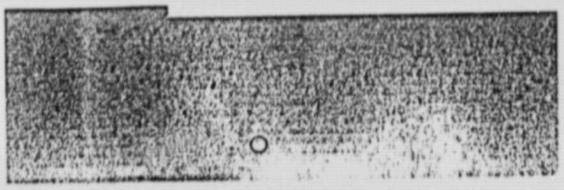

Mg X

JAN 7

Ne VII

Mg VIII

JAN 8

Ne VII

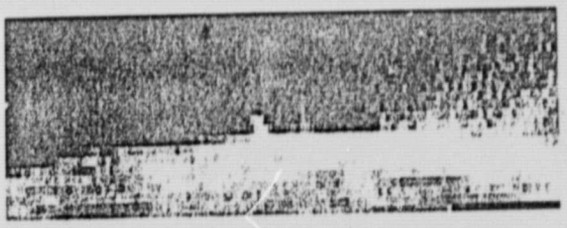

Mg VIII

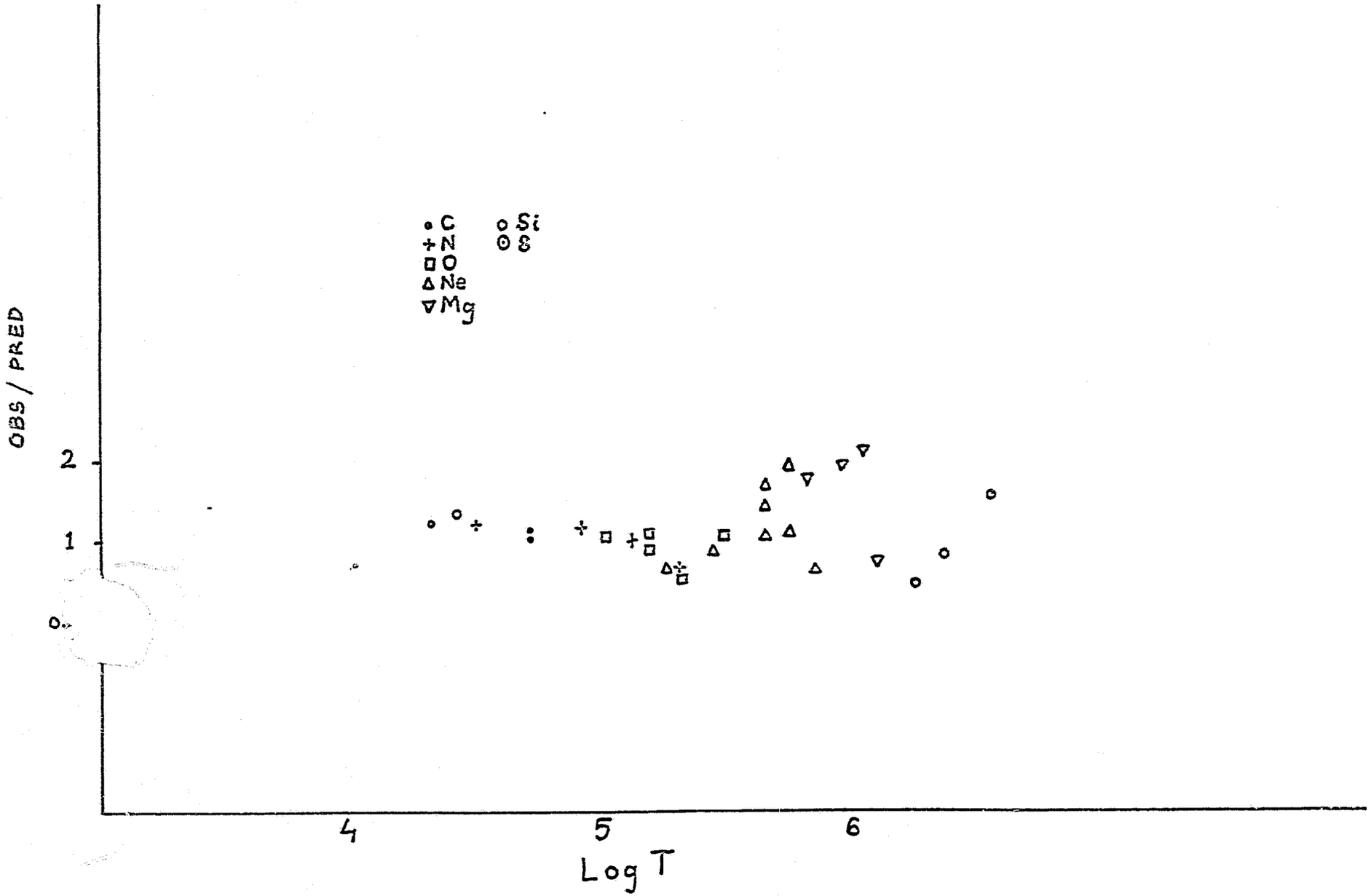
C
N
O
Ne
Mg
Si
S
OBS / PRED
2
1
0
4
5
6
Log T

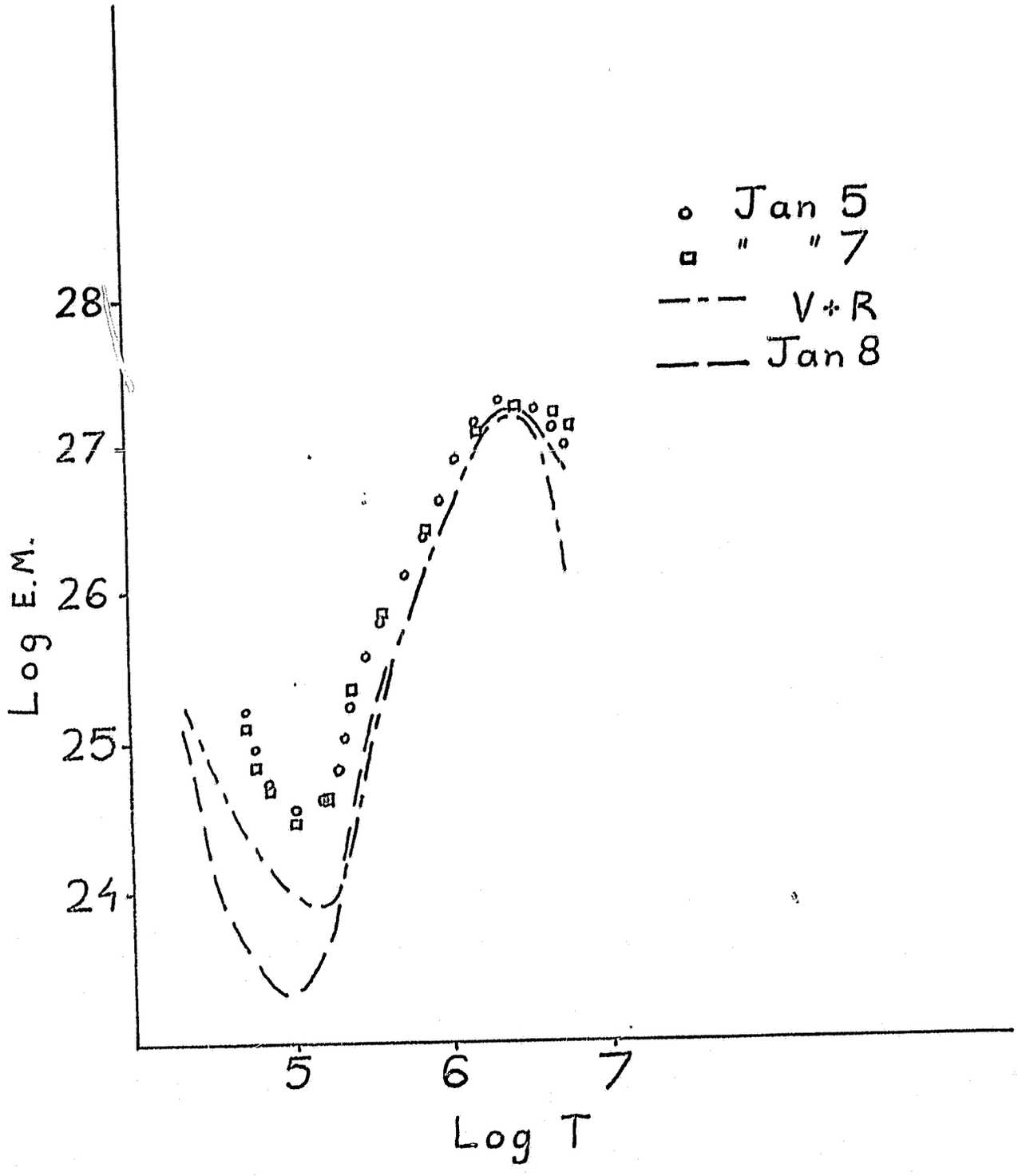
Jan 5
" " 7
V + R
Jan 8
28
27
26
25
24
Log E.M.
5
6
7
Log T

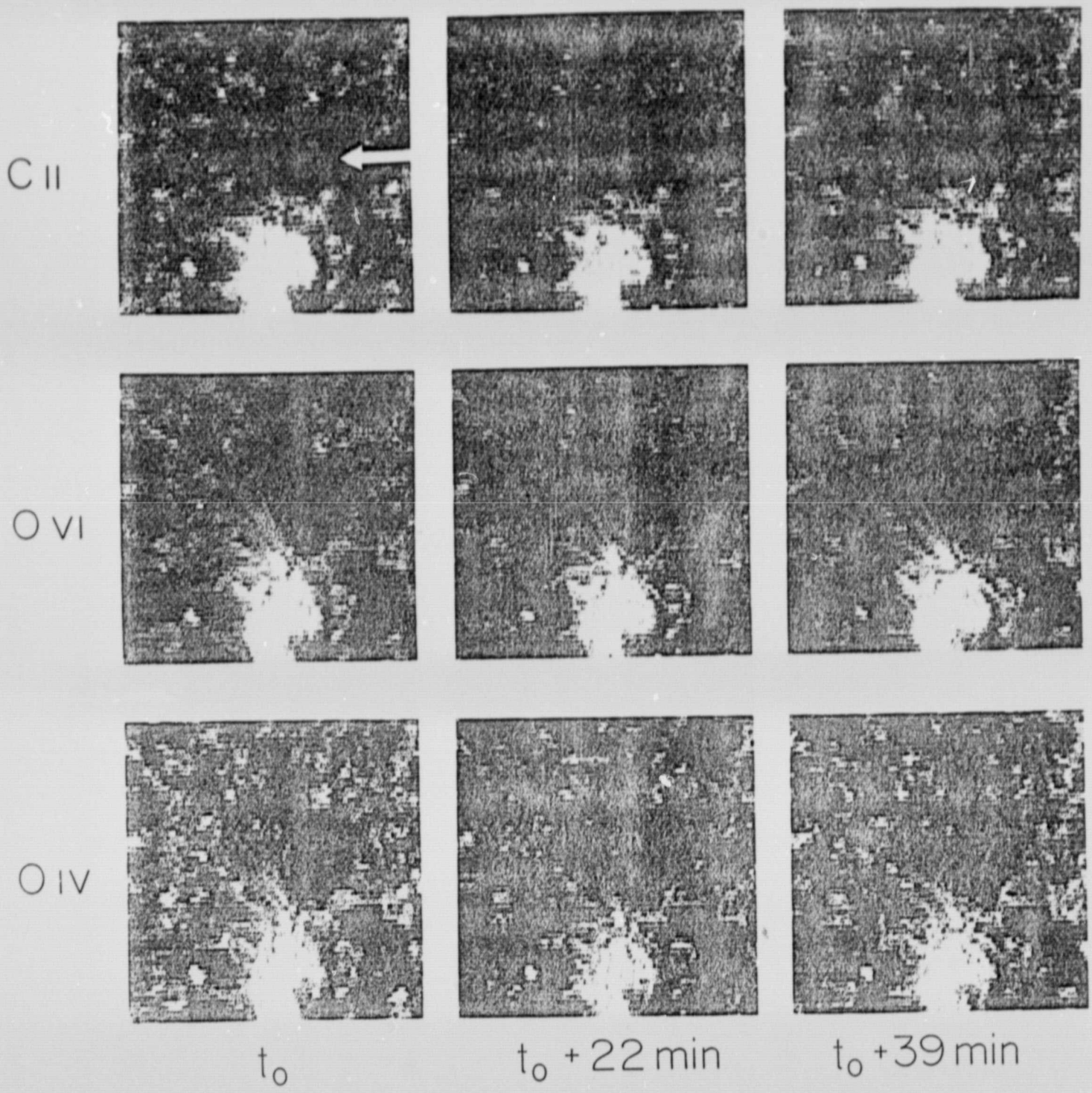
C II
O VI
O IV
t_o
t_o + 22 min
t_o + 39 min

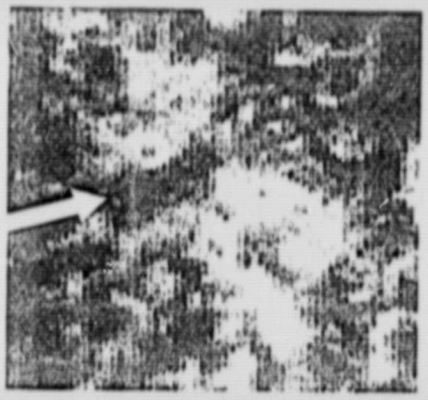

Ly α

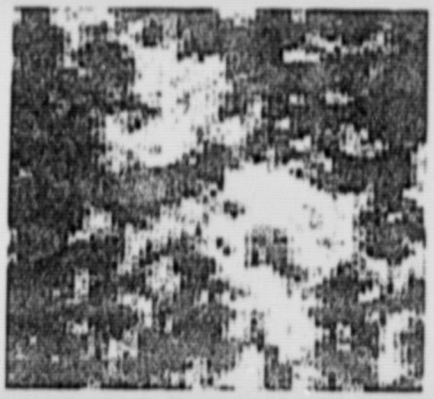

C II

C III

O IV

O VI

Mg X

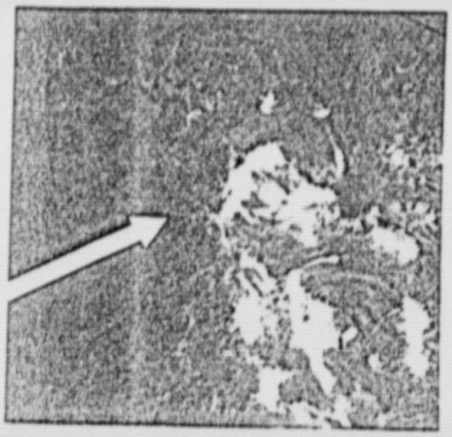

H α

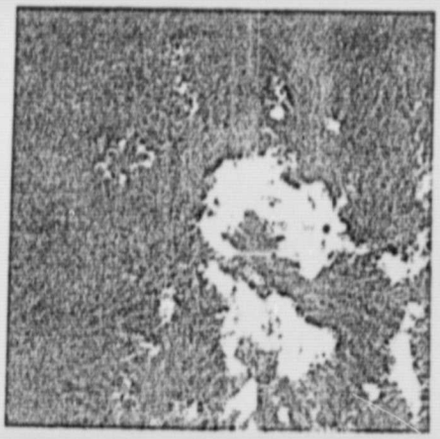

H α

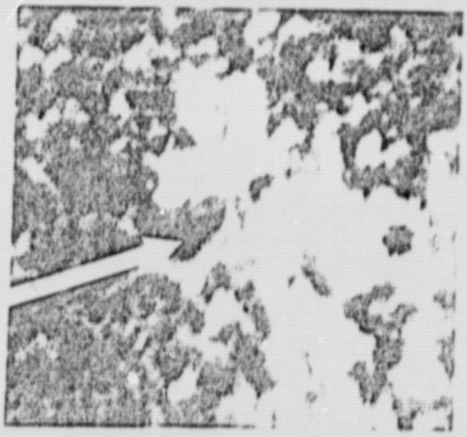

Ca K

Ly α

C II

C III

O IV

O VI

Mg X

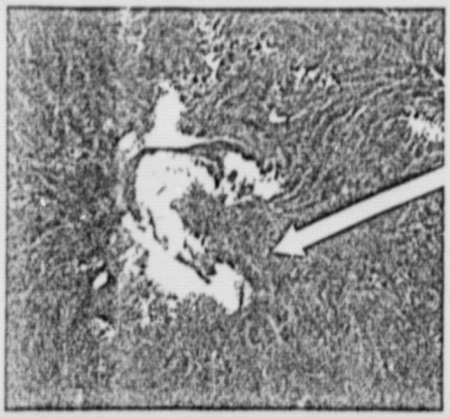

H α

H α

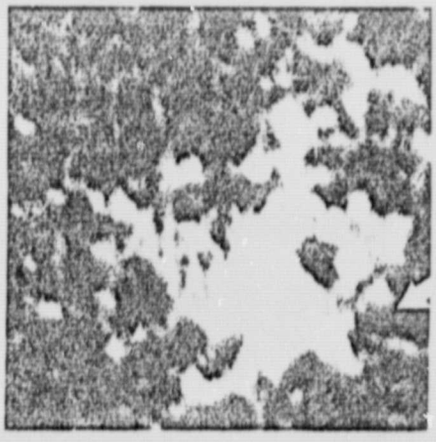

Ca K

Ly α

Ly C

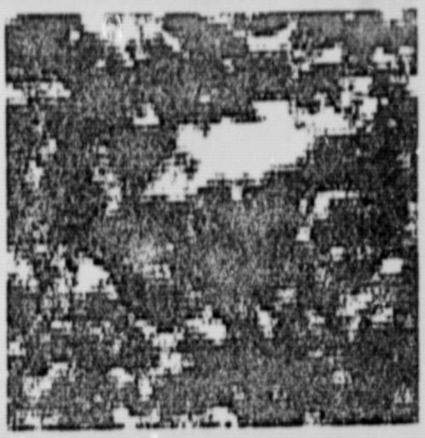

C II

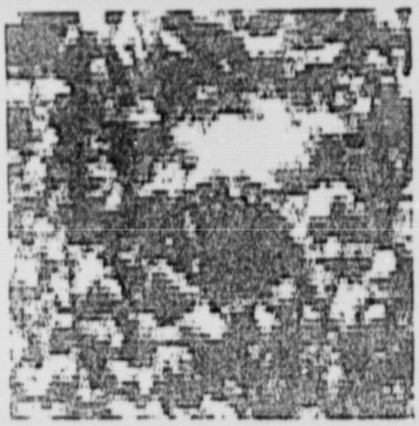

C III

O IV

O VI

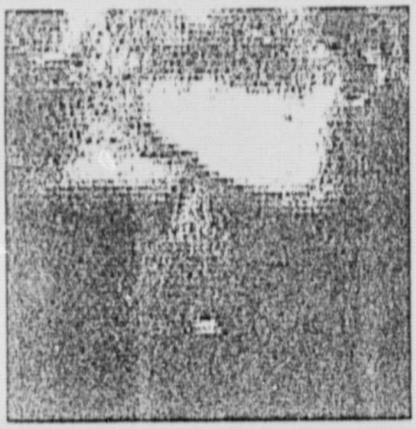

Mg X

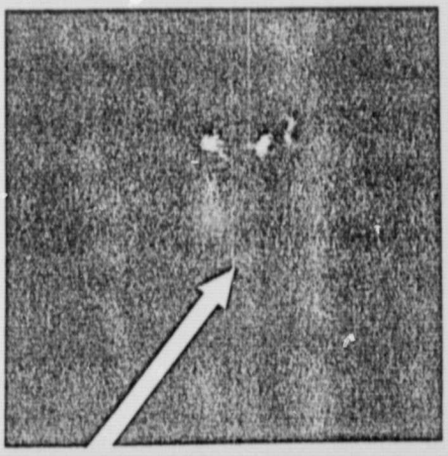

H α

Ca K

(a)

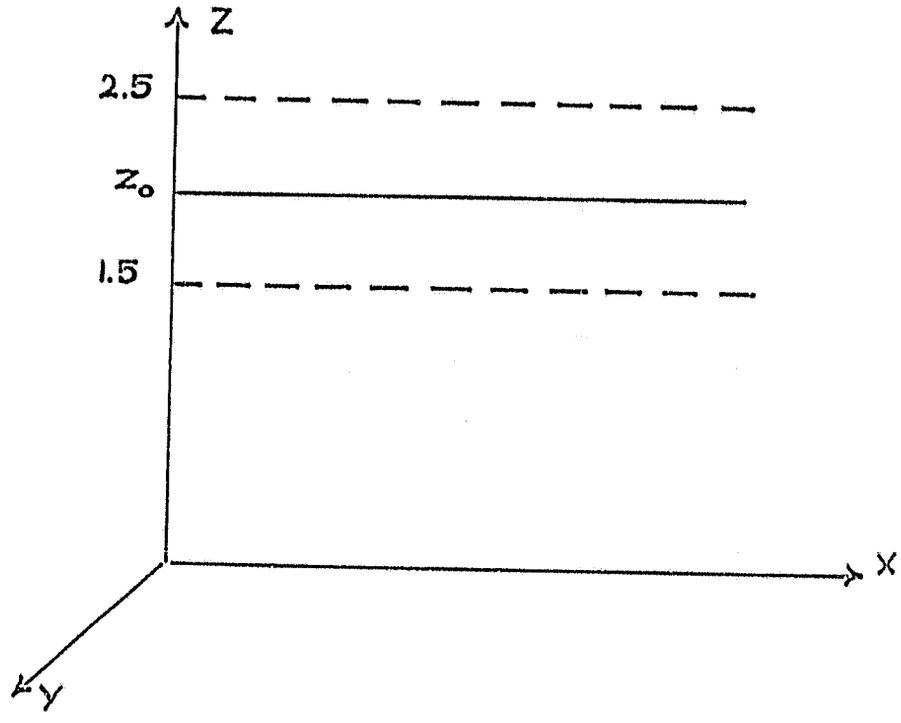

(b)

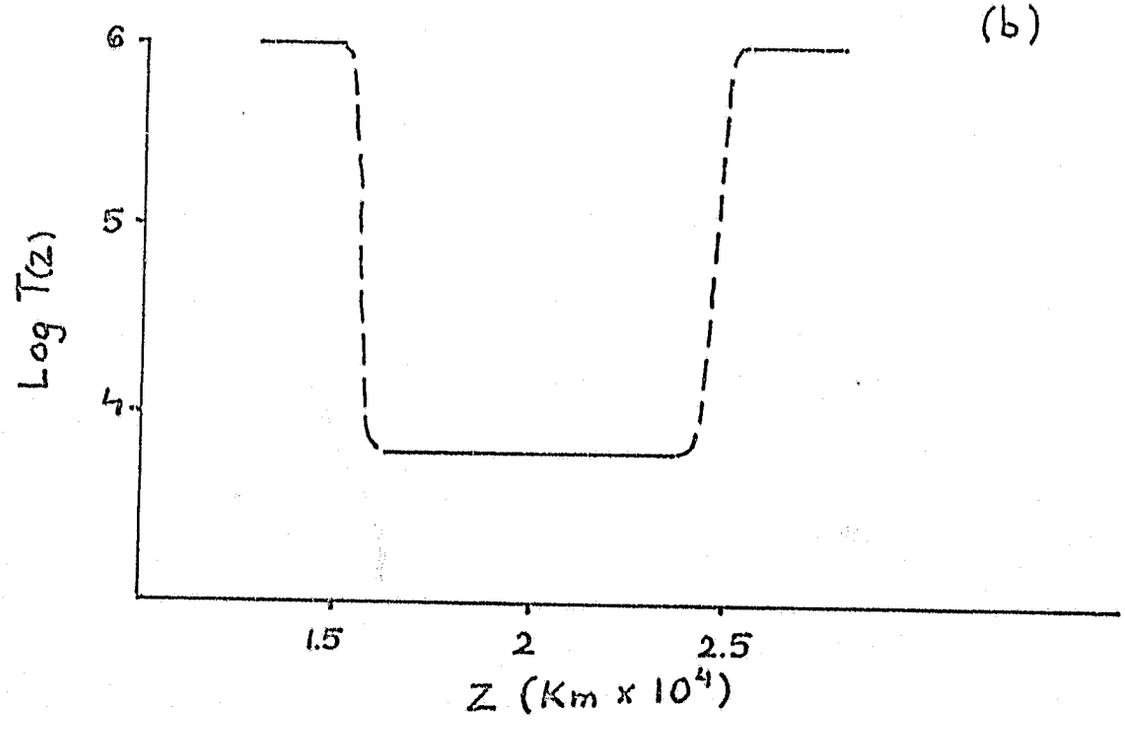

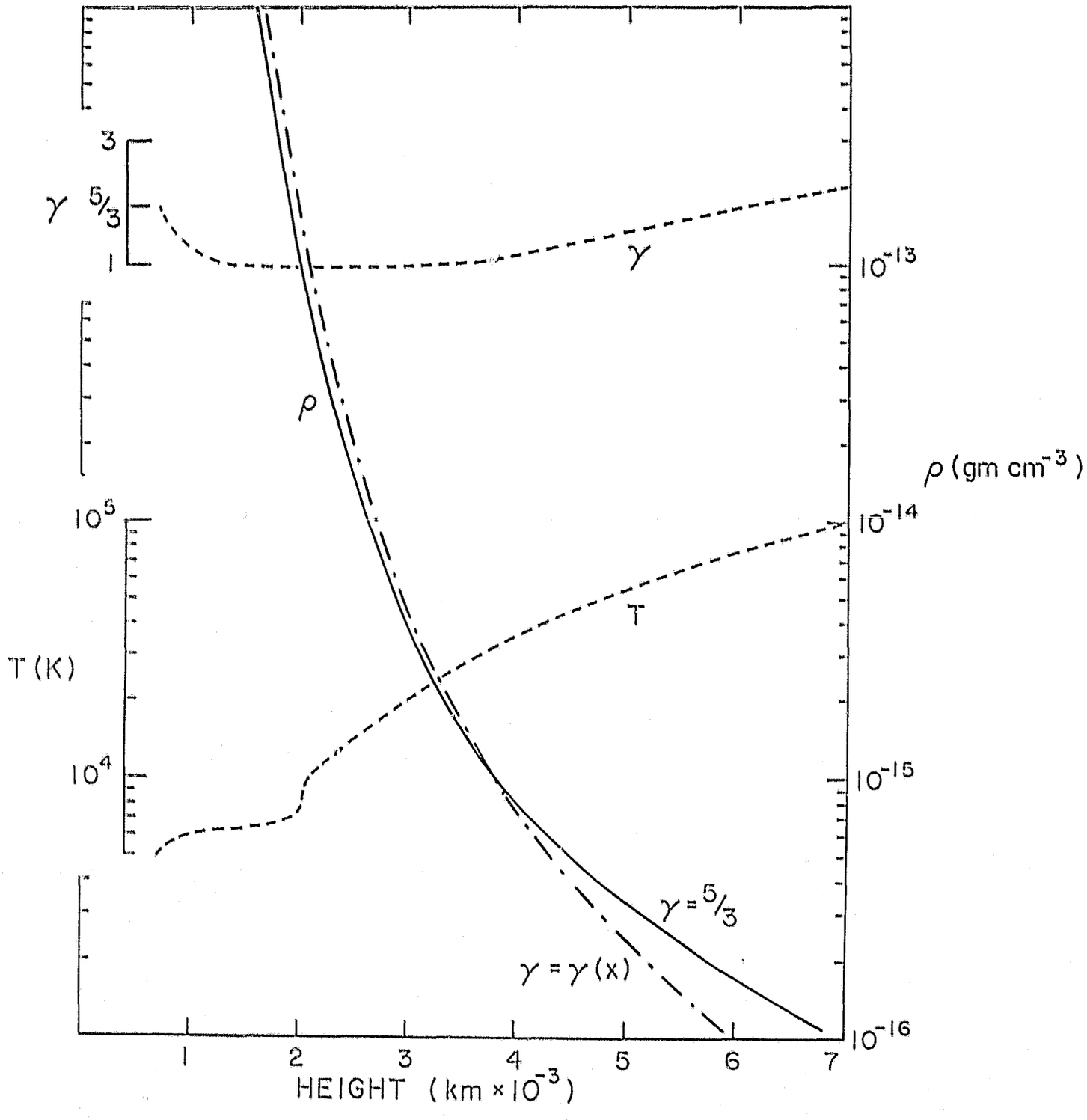
3
γ 5/3
1
γ
ρ
10^-13
10^-14
10^-15
10^-16
ρ (gm cm^-3)
10^5
10^4
T (K)
T
γ = 5/3
γ = γ(x)
1
2
3
4
5
6
7
HEIGHT (km × 10^-3)

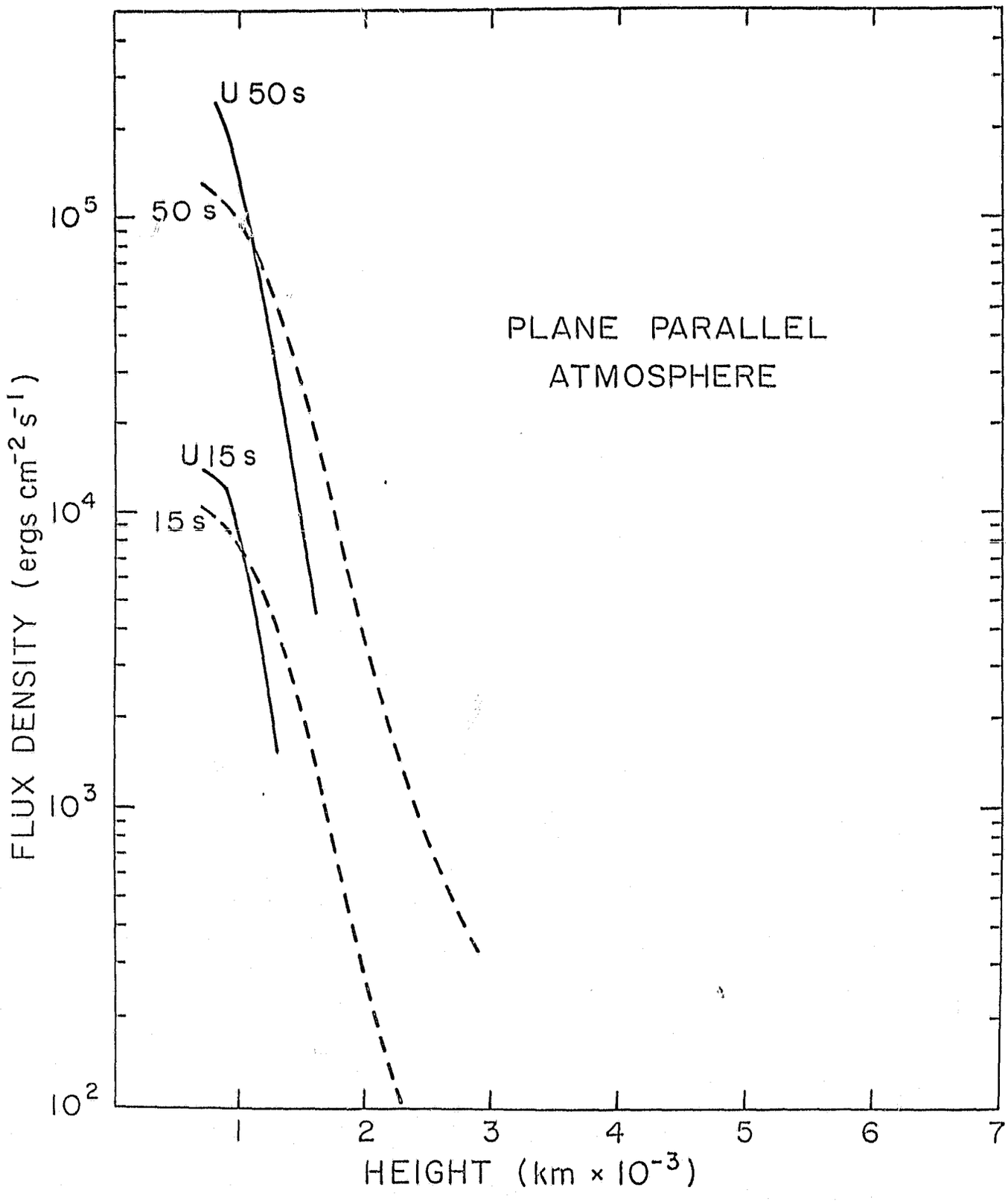
U 50 s
50 s
U 15 s
15 s
PLANE PARALLEL
ATMOSPHERE
FLUX DENSITY (ergs cm^{-2} s^{-1})
10^5
10^4
10^3
10^2
1
2
3
4
5
6
7
HEIGHT (km × 10^{-3})

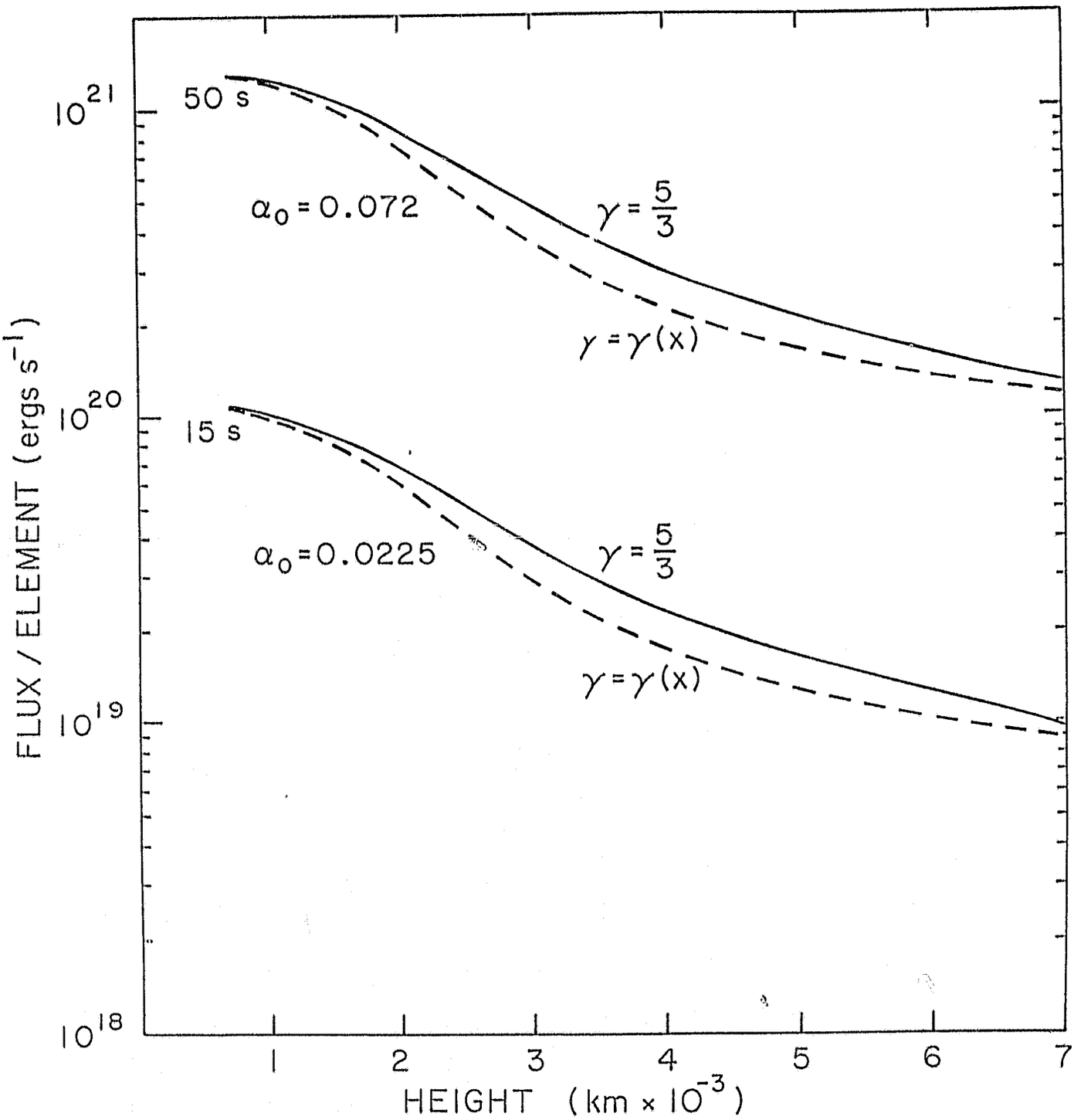
50 s
$\alpha_0 = 0.072$
$\gamma = \frac{5}{3}$
$\gamma = \gamma(x)$
15 s
$\alpha_0 = 0.0225$
$\gamma = \frac{5}{3}$
$\gamma = \gamma(x)$
10^{21}
10^{20}
10^{19}
10^{18}
FLUX / ELEMENT (ergs s^{-1})
1
2
3
4
5
6
7
HEIGHT (km $\times 10^{-3}$)

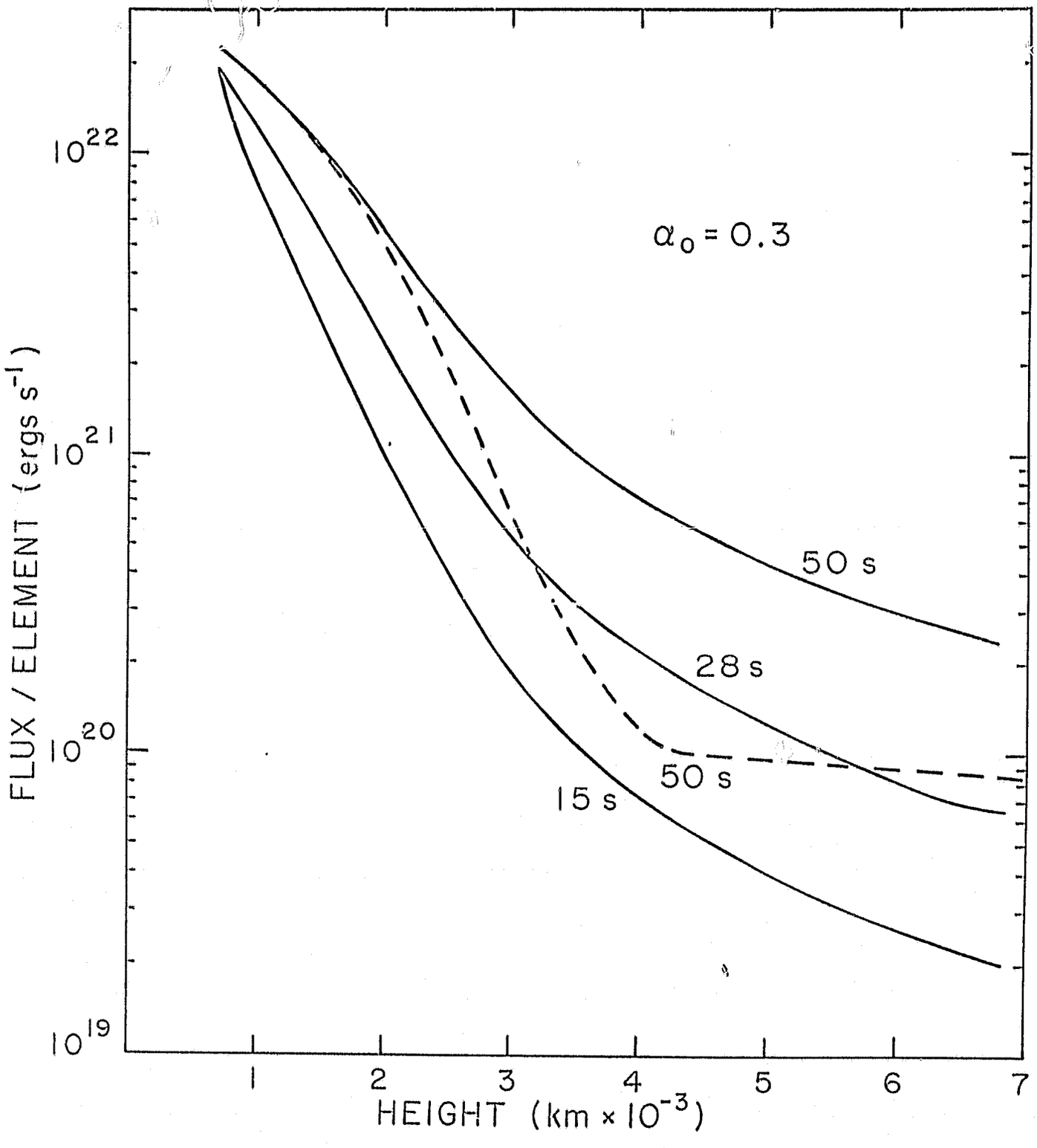
$\alpha_o = 0.3$
50 s
28 s
50 s
15 s
FLUX / ELEMENT (ergs s^{-1})
10^{22}
10^{21}
10^{20}
10^{19}
1
2
3
4
5
6
7
HEIGHT (km × 10^{-3})

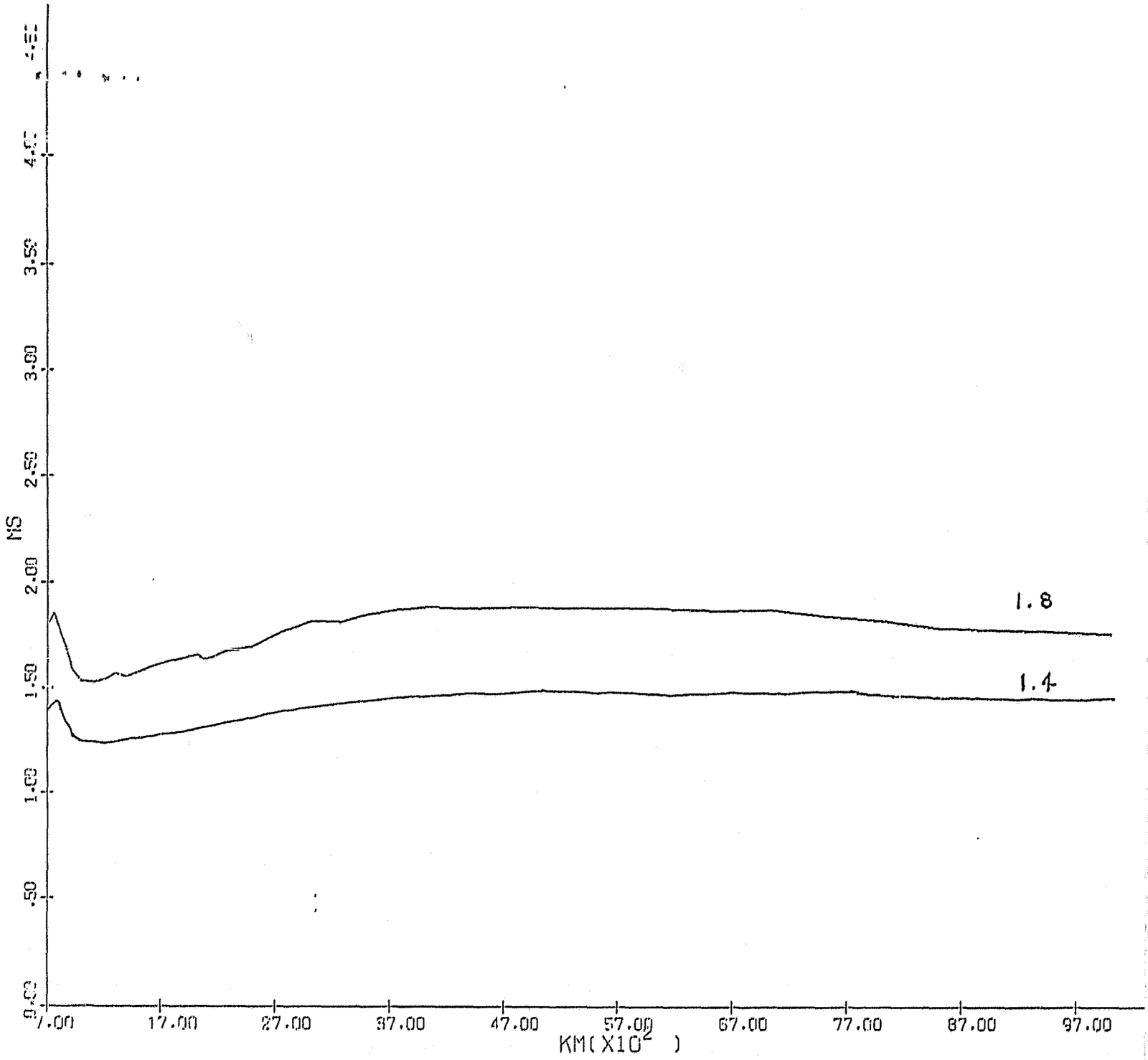
NS
2.00
1.50
.50
0.00
1.8
1.4
7.00
17.00
27.00
37.00
47.00
57.00
67.00
77.00
87.00
97.00
KM(X10²)

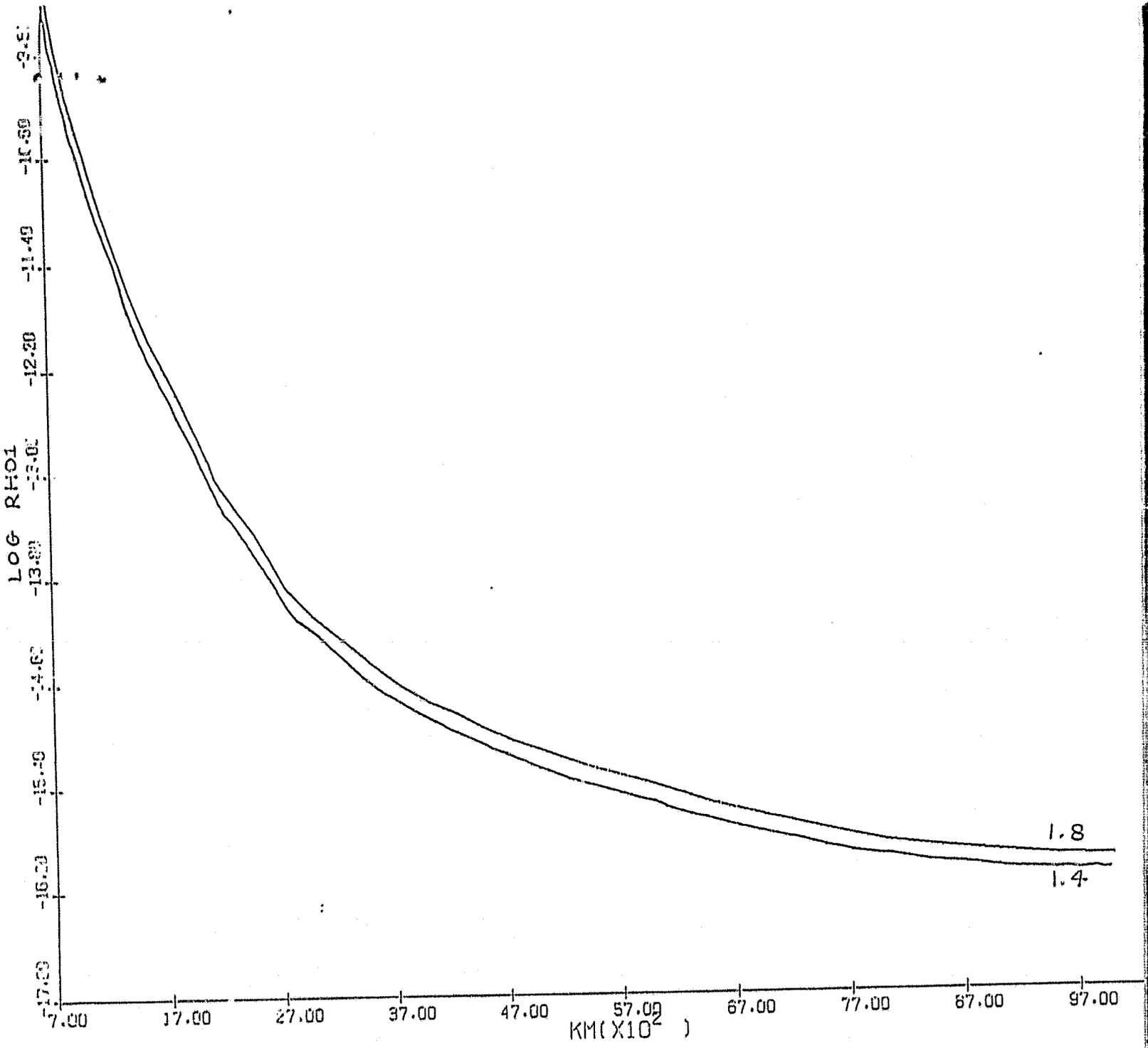
LOG RHO1
-10.59
-11.49
-12.39
-15.09
7.00
17.00
27.00
37.00
47.00
57.00
67.00
77.00
87.00
97.00
KM(X10²)
1.8
1.4

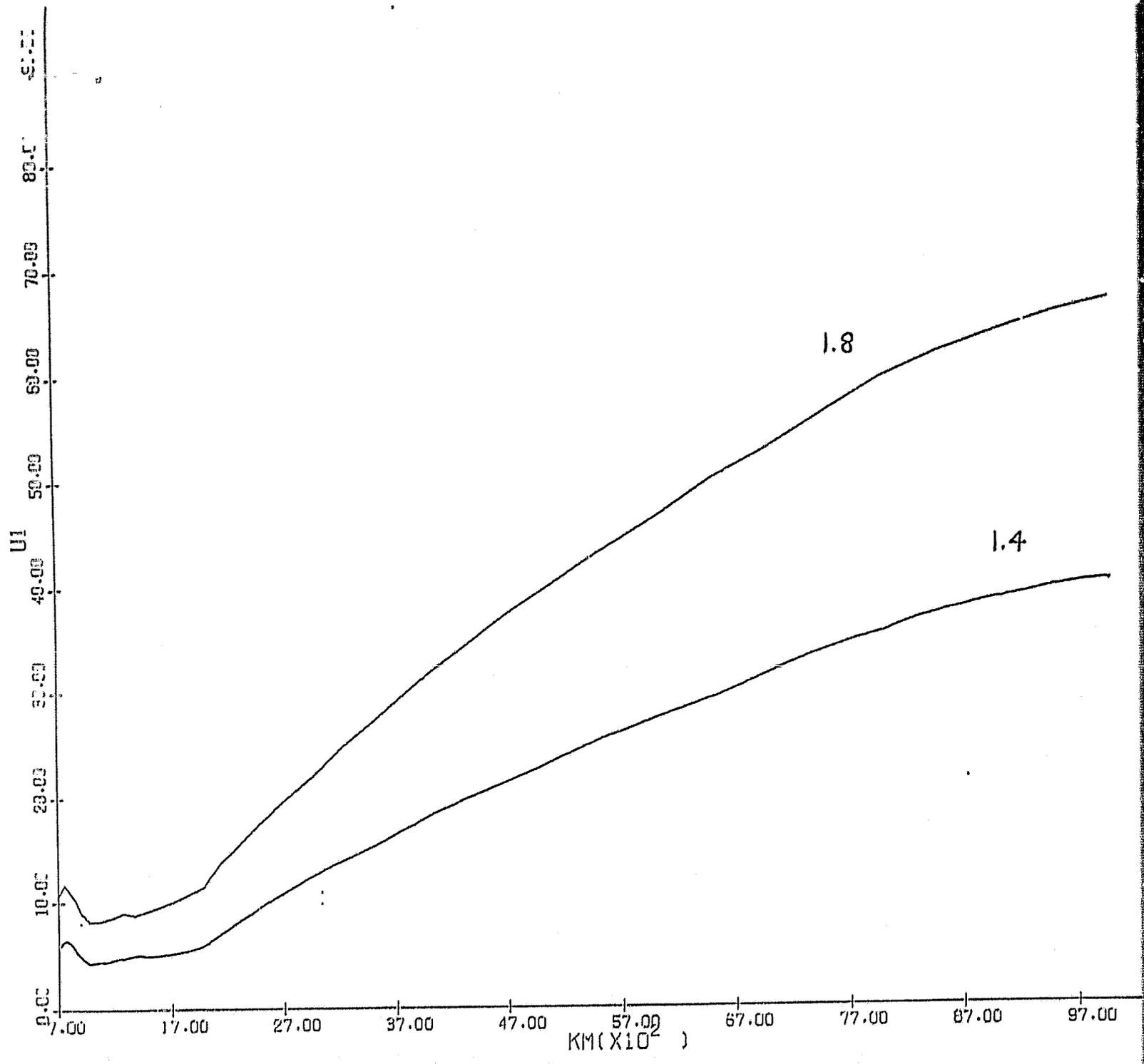
U1
70.00
60.00
50.00
40.00
23.00
10.00
0.00
1.8
1.4
7.00
17.00
27.00
37.00
47.00
57.00
67.00
77.00
87.00
97.00
KM(X10)

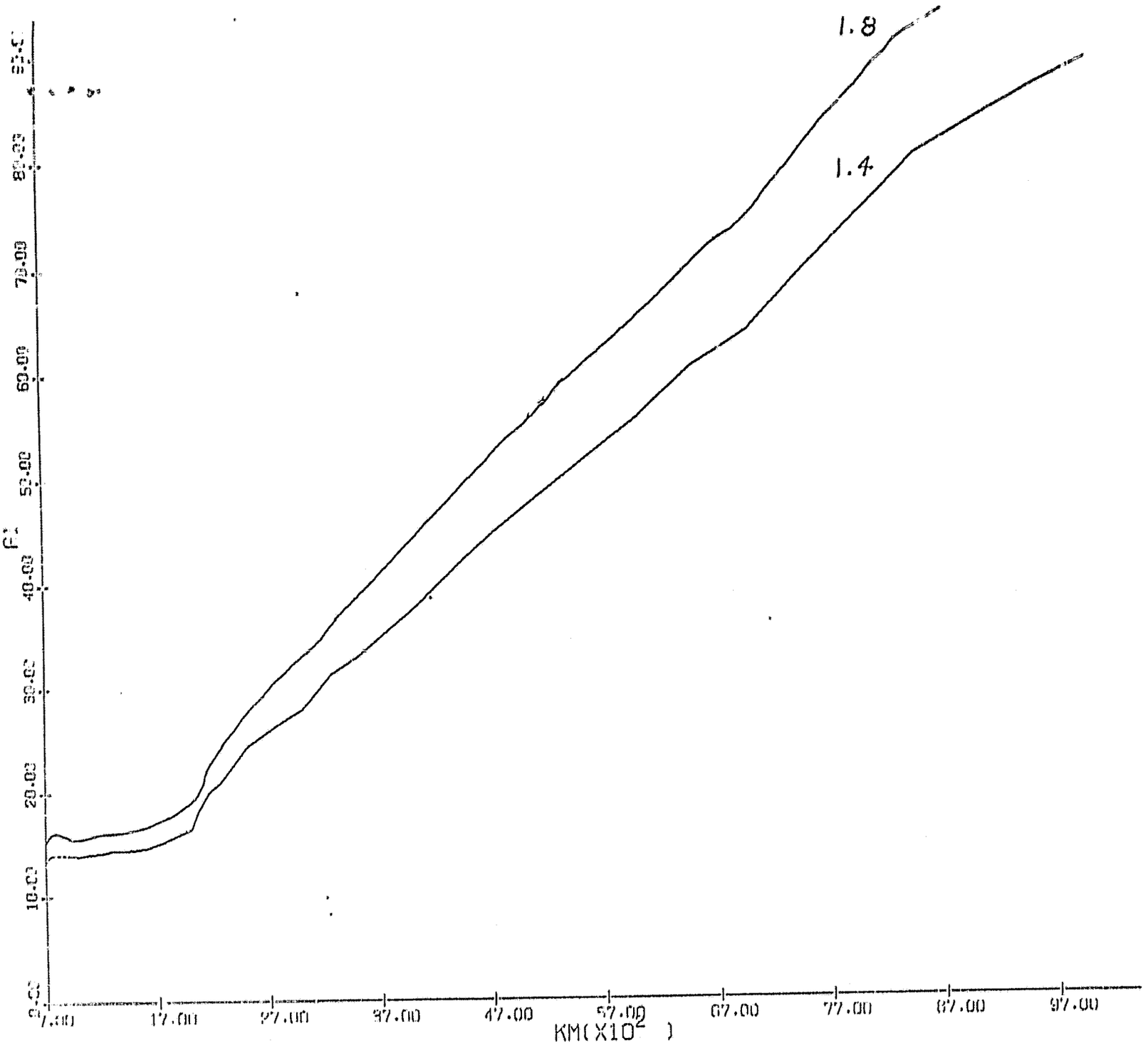
1.8
1.4
70.00
60.00
50.00
40.00
30.00
20.00
10.00
17.00
27.00
37.00
47.00
57.00
67.00
77.00
87.00
97.00
KM(X10²)